see commentary on page 907

# Slc26a11, a chloride transporter, localizes with the vacuolar $H^+$-ATPase of A-intercalated cells of the kidney

Jie Xu[1,2,3,4], Sharon Barone[1,2,3,4], Hong Li[1,2,3,4], Shannon Holiday[1,2,3,4], Kamyar Zahedi[1,2,3,4] and Manoocher Soleimani[1,2,3,4]

*[1]Research Services, Veterans Affairs Medical Center, Cincinnati, Ohio, USA; [2]Department of Medicine, University of Cincinnati, Cincinnati, Ohio, USA; [3]Department of Orthodontics, University of Florida, Gainesville, Florida, USA and [4]Center on Genetics of Transport and Epithelial Biology, University of Cincinnati, Cincinnati, Ohio, USA*

**Chloride has an important role in regulating vacuolar $H^+$-ATPase activity across specialized cellular and intracellular membranes. In the kidney, vacuolar $H^+$-ATPase is expressed on the apical membrane of acid-secreting A-type intercalated cells in the collecting duct where it has an essential role in acid secretion and systemic acid base homeostasis. Here, we report the identification of a chloride transporter, which co-localizes with and regulates the activity of plasma membrane $H^+$-ATPase in the kidney collecting duct. Immunoblotting and immunofluorescent labeling identified Slc26a11 (~72 kDa), expressed in a subset of cells in the collecting duct. On the basis of double-immunofluorescent labeling with AQP2 and identical co-localization with $H^+$-ATPase, cells expressing Slc26a11 were deemed to be distinct from principal cells and were found to be intercalated cells. Functional studies in transiently transfected COS7 cells indicated that Slc26a11 (designated as kidney brain anion transporter (KBAT)) can transport chloride and increase the rate of acid extrusion by means of $H^+$-ATPase. Thus, Slc26a11 is a partner of vacuolar $H^+$-ATPase facilitating acid secretion in the collecting duct.**

*Kidney International* (2011) **80,** 926–937; doi:10.1038/ki.2011.196; published online 29 June 2011

KEYWORDS: cell and transport physiology; immunohistochemistry; intracellular pH; ion transport; physiology

**Correspondence:** *Manoocher Soleimani, Center on Genetics of Transport and Epithelial Biology and Department of Internal Medicine, University of Cincinnati, 231 Albert Sabin Way, MSB 6312, Cincinnati, Ohio, USA. E-mail: Manoocher.Soleimani@uc.edu*

**Received 26 January 2011; revised 20 April 2011; accepted 26 April 2011; published online 29 June 2011**

SLC26(human)/Slc26(mouse) isoforms belong to a conserved family of anion transporters and are expressed in various tissues and organs, with some paralogs displaying specific tissue, cell, or subcellular expression pattern.[1–8] SLC26 isoforms can transport various anions, including chloride, sulfate, bicarbonate, and oxalate, with variable specificity.[9,10] Several SLC26A members function as chloride/bicarbonate exchangers. These include SLC26A3 (DRA), SLC26A4 (pendrin), SLC26A6 (PAT1), SLC26A7, and SLC26A9.[11–18] SLC26A7 and SLC26A9 can also function as chloride channels.[18–21] Several SLC26 isoforms can transport oxalate, including SLC26A6 (PAT1), A7, A8, and A9.[22–26] SLC26 family members share a signature sequence on their C-terminal domain, which is referred to as sulfate transporter and anti-sigma factor domain and has an important role in transport function.[1–10]

At present, little is known about SLC26A11, other than that its mRNA is expressed in several tissues including the placenta, kidney, and venules, and can transport sulfate.[8] No studies have examined the cellular distribution and subcellular localization of SLC26A11 in the kidney or in any other tissues. Furthermore, the affinity of SLC26A11 for chloride transport or $Cl^-/HCO_3^-$ exchange, and its ability to facilitate any biological process remain unknown.

Vacuolar $H^+$-ATPase is expressed in the plasma membrane of specialized cells such as osteoclast and kidney collecting duct intercalated cells (review).[27,28] The secretion of acid through $H^+$-ATPase into the lumen of the kidney collecting duct, and connecting, distal convoluted and proximal tubule has an essential role in systemic acid base homeostasis.[29–31] It is well established that chloride has an important role in regulating the activity of V $H^+$-ATPase expressed in the cellular and intracellular membranes.[32–35] The effect of chloride is likely mediated through two distinct mechanisms. The first is believed to be through the dissipation of a potential difference when chloride is secreted electrogenically, whereas the second is through a direct, specific stimulatory role that has been less well characterized.[32–36]

Our studies demonstrate that the expression of Slc26a11 in the kidney is exclusively limited to the collecting duct, with remarkable co-localization with $H^+$-ATPase in intercalated cells. We further demonstrate that Slc26a11 mediates the transport of chloride and can facilitate acid extrusion through $H^+$-ATPase. We propose that Slc26a11 is a functional partner of $H^+$-ATPase and regulates acid secretion in the collecting duct.

## RESULTS

### Expression of Slc26a11

We first examined the distribution of Slc26a11 mRNA in mouse tissues. Figure 1a is a northern hybridization indicating the expression of Slc26a11 in multiple tissues, with abundant mRNA levels in the brain and kidney, followed by the distal colon. Next, reverse transcription-PCR experiments were performed on RNA isolated from various kidney zones to examine the zonal distribution of Slc26a11. The results demonstrated the expression of Slc26a11 in the cortex and medulla of mouse kidney (Figure 1b) as verified by sequencing of the single 1.2-kb band. Northern hybridization verified that Slc26a11 mRNA was abundantly expressed in the cortex and medulla (data not shown). This pattern of expression is distinct from Slc26a6 (PAT1), which is abundantly expressed in the cortex but is absent in the medulla, and Slc26a7 (PAT2), which is expressed in the medulla but not in the cortex.[16,17]

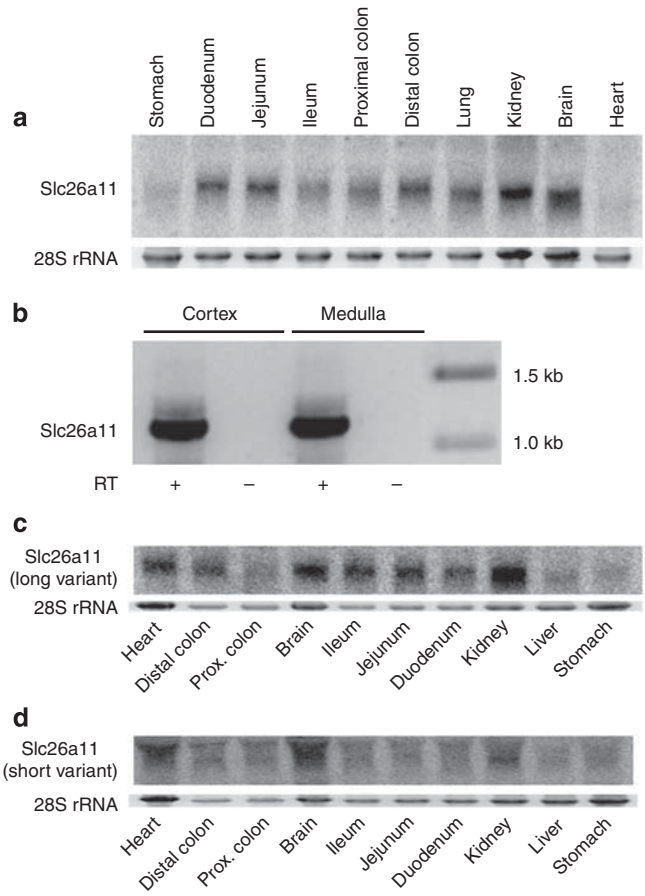


**Figure 1 | Slc26a11 distribution in mouse tissues and kidney.** (**a**) Tissue distribution of Slc26a11. Slc26a11 transcript size was 2.0 kb. Slc26a11 was detected abundantly in the kidney and brain, followed by upper small intestine and distal colon. 28S rRNA levels are shown as constitutive controls. In all, 30 μg of RNA was loaded on each lane. (**b**) Kidney expression of Slc26a11 by RT-PCR. A representative ethidium bromide staining of agarose gel demonstrates a PCR product of expected size (1200 bp) in the cortex and medulla. (**c**) Tissue distribution of the Slc26a11 long variant. The long Slc26a11 variant is expressed in the kidney and other epithelial cells, with lower levels in the brain. (**d**) Tissue distribution of the Slc26a11 short variant. The short Slc26a11 variant is predominantly expressed in the brain, with lower levels in other tissues. RT-PCR, reverse transcriptase-PCR.

Mouse Slc26a11 has two distinct variants (GenBank accession numbers: AF345196 and BC132493) with the long variant having an additional 170 amino acids (aa) on its N-terminal end. In the next series of experiments, we examined the tissue distribution of long and short variants using variant-specific radiolabeled DNA probes (Materials and Methods). Figure 1c is a northern hybridization and shows that the long variant is predominantly expressed in the kidney and in several other epithelial tissues, including the brain. However, the short variant is predominantly expressed in the brain with lower levels in the kidney (Figure 1d). Given its abundant expression in the kidney and brain and its functional activity as an anion transporter (see below), we wish to designate Slc26a11 as KBAT (kidney brain anion transporter).

### Immunoblotting and immunofluorescent labeling of Slc26a11 (KBAT) in the kidney

Using an antibody generated against the mouse Slc26a11, a 72-kDa band was detected in microsomal membrane proteins from the renal medulla (Figure 2a, left panel). The labeling of the 72-kDa band was completely prevented with the pre-adsorbed immune serum (Figure 2a, left panel). To examine the specificity of the Slc26a11 antibody further, COS7 cells were transfected with the full-length Slc26a11 cDNA, labeled with Slc26a11 antibodies, and co-labeled with phalloidin-tetramethylrhodamine, a marker of the actin cytoskeleton. Images were taken on a Zeiss LSM510 confocal microscope (Zeiss, Thornwood, NY) and analyzed as before.[17] As indicated (Figure 2a, right panel), the Slc26a11 antibodies specifically label the plasma membrane of cells transfected with the Slc26a11 cDNA but not with the empty vector.

To determine the cellular distribution and subcellular localization of KBAT, immunofluorescent staining with the purified immune serum was performed in the kidney. As shown in Figure 2bA–C, low-magnification images detected the expression of KBAT in a subset of cells in the collecting duct in the cortex, outer medulla, and inner medulla. As demonstrated in images with higher magnification, the labeling of KBAT in the cortex was detected on either the apical or the basolateral membrane domains in collecting duct cells (Figure 2cA), whereas the labeling of KBAT in the outer medullary collecting duct and inner medullary collecting duct was exclusively limited to the apical membrane (Figure 2cB and C). The labeling with KBAT

antibodies was specific, as pre-adsorbed immune serum failed to detect any labeling in the kidney (Figure 2d).

To determine the identity of Slc26a11-expressing cells, double-immunocytochemical staining with antibodies against Slc26a11 and aquaporin 2 (AQP2), which is exclusively expressed on the apical membrane of principal cells, was performed. As shown in Figure 3aA (the cortex, outer medulla, and inner medulla), KBAT (left) and AQP2 (right) clearly localized to two distinct cell populations in the cortical collecting duct (Figure 3aA), outer medullary

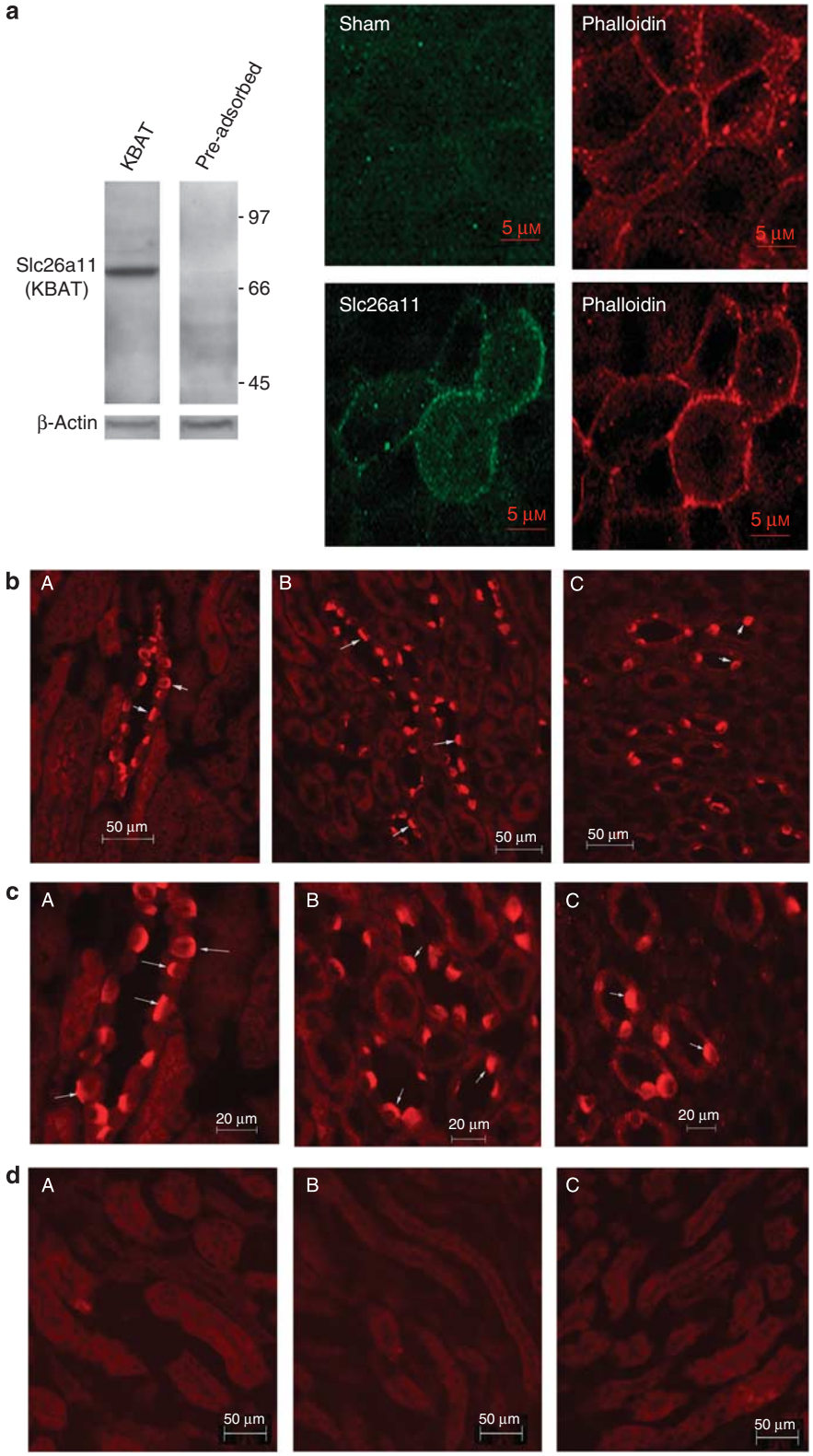

collecting duct (Figure 3aB), and inner medullary collecting duct (Figure 3aC) (merged images in the middle), clearly demonstrating that cells expressing KBAT (Slc26a11) are distinct from principal cells. An obvious conclusion from these studies is that Slc26a11 (KBAT) is located in intercalated cells in the collecting duct. To examine this issue

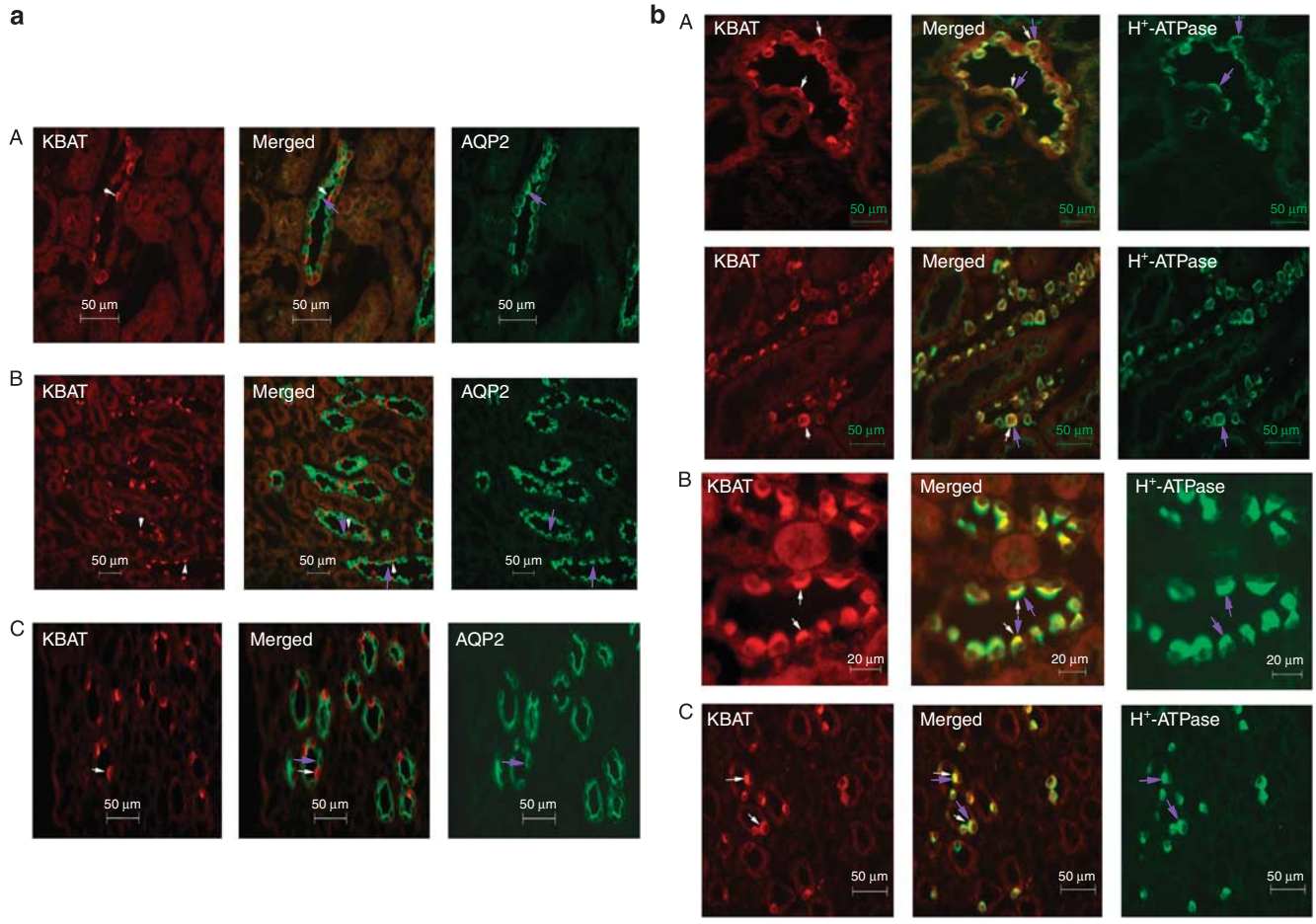


**Figure 3 | Immunofluorescent double staining of KBAT with AQP2 or H$^+$-ATPase.** (**a**) Double immunofluorescent labeling of KBAT and aquaporin 2 (AQP2) in the kidney. (A) Cortex (top). Immunostaining in the kidney indicated that the distribution of AQP2 (right, purple arrow) and Slc26a11 (left, white arrow) corresponded to two distinct cell subtypes in the CCD when dual images were acquired (middle). (B and C) Outer medulla (B) and inner medulla (C). Immunostaining in the kidney indicated that the distribution of AQP2 (right, purple arrows) and Slc26a11 (left, white arrows) corresponded to two distinct cell subtypes in the OMCD (B) and IMCD (C) when dual images were acquired (middle), indicating that Slc26a11 is localized on the apical membrane of cells distinct from principal cells. (**b**) Double-immunofluorescent labeling of KBAT and H$^+$-ATPase in the kidney. (A) Cortex. Two sets of data (top and bottom panels) are shown in panel (**b**A). As shown, Slc26a11 (left, white arrows) and H$^+$-ATPase (right, purple arrows) demonstrate remarkably identical localization patterns in the cortical collecting duct when merged images are acquired (middle). Slc26a11 co-localizes with H$^+$-ATPase on the apical membrane of A-intercalated cells and on the basolateral membrane of B-intercalated cells in the CCD. (B and C) Outer medulla (**b**B) and inner medulla (**b**C). In the OMCD (**b**B) and IMCD (**b**C), Slc26a11 (left, white arrows) co-localizes with H$^+$-ATPase (right, purple arrows) exclusively on the apical membrane of A-intercalated cells (merged image in the middle). CCD, cortical collecting duct; IMCD, inner medullary collecting duct; KBAT, kidney brain anion transporter; OMCD, outer medullary collecting duct.

**Figure 2 | Immunolocalization of Slc26a11 (KBAT) in the kidney.** (**a**) Specificity of KBAT antibodies and immunoblotting of KBAT in the kidney. Left panel: with the use of the antibody generated against the mouse Slc26a11, a ~72-kDa band was detected in the kidney medulla. Labeling of the 72-kDa band was completely prevented with the pre-adsorbed immune serum. Right panel: KBAT antibody specifically labels the plasma membrane of COS7 cells transfected with Slc26a11 cDNA. Top: cells transfected with empty vector (sham), bottom: cells transfected with Slc26a11 cDNA. Cells were labeled with KBAT antibodies (Slc26a11, left) and co-labeled with phalloidin (right), as a marker of the actin cytoskeleton. (**b**) Immunofluorescent labeling with KBAT antibodies (low magnification). Low magnification of Slc26a11 labeling in the cortex (A, left), outer medulla (B, middle), and the inner medulla (C, right). (**c**) Immunofluorescent labeling with KBAT antibodies (high magnification). Higher magnifications of Slc26a11 labeling in the cortex (A, left), outer medulla (B, middle), and the inner medulla (C, right). Results clearly demonstrate that in the cortex, the labeling of KBAT was detected on the apical or basolateral membrane domains in the CCD (arrows). In the medulla, KBAT was only detected on the apical membrane domain of a subset of cells in OMCD (B) and IMCD (C) (arrows). (**d**) Immunolabeling with pre-adsorbed immune serum. No labeling was detected with the pre-adsorbed immune serum in the cortex (A) and in the medulla (B and C). CCD, cortical collecting duct; IMCD, inner medullary collecting duct; KBAT, kidney brain anion transporter; OMCD, outer medullary collecting duct.

further, double-immunofluorescent labeling using KBAT and $H^+$-ATPase antibodies was performed. As demonstrated, merged images display remarkably identical co-localization of KBAT with $H^+$-ATPase along the length of the collecting duct (Figure 3bA–C). As shown, KBAT and $H^+$-ATPase co-localize on the apical membrane of A-intercalated cells and on the basolateral membrane of B-intercalated cells in the cortical collecting duct (Figure 3bA). Some cells display co-localization of KBAT and $H^+$-ATPase on the apical and basolateral membranes of the same cells (Figure 3bA). These latter cells most likely represent non-A-, non-B-intercalated cells, based on the reported $H^+$-ATPase expression pattern. The co-localization of $H^+$-ATPase and KBAT in the outer medullary collecting duct (Figure 3bB) and the initial portion of inner medullary collecting duct (Figure 3bC) was exclusively detected on the apical membrane of A-intercalated cells, consistent with the loss of non-A-intercalated cells in medullary collecting ducts. These results clearly demonstrate the co-localization of Slc26a11 (KBAT) with $H^+$-ATPase in the collecting duct.

#### Functional examination of Slc26a11 (KBAT)

To ascertain the functional identity of KBAT, COS7 cells were transiently transfected as described in the 'Materials and Methods' section. We first tested whether Slc26a11 has the ability to transport chloride. Toward this end, 24-well plates transfected with KBAT cDNA were used for $^{36}Cl$ influx and efflux experiments as described in the 'Materials and Methods' section. As shown in Figure 4a, cells transiently transfected with Slc26a11 cDNA demonstrated increased uptake of $^{36}Cl$ vs mock-transfected cells ($P<0.02$, $n=6$). The 10-min influx of $^{36}Cl$ was significantly inhibited by 0.5 mmol/l 4,4′-Diisothiocyano-2,2′-stilbenedisulfonic acid (DIDS) in transfected cells (Figure 4a). We next examined the role of Slc26a11 in chloride efflux across the cell membrane in the absence or presence of external chloride. In the absence of extracellular chloride (all chloride salts were replaced with gluconate salts), Slc26a11-expressing cells demonstrated significant $^{36}Cl$ efflux relative to mock-transfected cells, when an outwardly directed potassium gradient which causes depolarization (extracellular $K=1$ mmol/l) was imposed, as shown in Figure 4b. In the presence of extracellular chloride (100 mmol/l $Cl^-$), the efflux of $^{36}Cl$ was significantly increased in Slc26a11-transfected vs mock-transfected cells ($P<0.01$, $n=6$) (Figure 4b). This $(Cl)_o/(^{36}Cl)_i$ exchange-mediated efflux was >2-fold higher relative to the absence of external chloride (Figure 4b). These results indicate that KBAT can function as an anion exchanger and as an electrogenic chloride-extruding pathway.

To examine the effect of membrane potential alteration on KBAT, $^{36}Cl$ efflux experiments were carried out under voltage-clamped conditions using valinomycin, a $K^+$-specific ionophore, and a $K^+$-rich solution and compared with a low $K^+$ extracellular solution. The efflux of $^{36}Cl$ was assayed in the presence or absence of chloride in the external solution. As shown in Figure 4c (left panel), in the absence of the external chloride but in the presence of valinomycin and $K^+$-rich solution, $^{36}Cl$ efflux in KBAT-transfected cells was significantly inhibited vs outwardly directed K gradient, and was not different relative to non-transfected cells ($n=6$, $P>0.05$). These results strongly suggest that the unidirectional chloride efflux (likely mediated through a conductive pathway) was regulated by membrane potential and is abrogated under voltage-clamped conditions. However, the efflux of $^{36}Cl$ in the presence of external chloride was only partially inhibited under voltage-clamped conditions in KBAT-transfected cells ($n=6$, $P<0.05$ vs mock-transfected cells; Figure 4c, right panel), indicating that the KBAT-mediated anion exchange pathway is in a large part independent of membrane potential alteration. The $^{36}Cl$ efflux in the presence or absence of extracellular chloride was significantly inhibited by 0.5 mmol/l DIDS.

Given the ability of KBAT to function as an anion exchanger (Figure 4b and c), we sought to determine whether KBAT could function in the $Cl^-/HCO_3^-$ exchange mode. Toward this end, COS7 cells were plated on coverslips and transiently transfected with KBAT cDNA. After 48 h, cells were loaded with the pH-sensitive dye BCECF (2′,7′-bis-(2-carboxyethyl)-5-(and-6)-carboxyfluorescein) and their intracellular pH ($pH_i$) was monitored as described in the 'Materials and Methods' section. Our results demonstrated that in the presence of $CO_2/HCO_3^-$ in the solutions, sequential switching of the perfusate to chloride-free and chloride-containing solutions induced a significant $pH_i$ alteration in KBAT-transfected cells relative to mock-transfected cells (Figure 4d). The summation of six separate coverslips showed that in the presence of $CO_2/HCO_3^-$ in the media, the rate of intracellular alkalinization in response to chloride removal was $0.13\pm0.015$ pH/min in KBAT-transfected and $0.04\pm0.007$ in mock-transfected cells ($P<0.02$, $n=6$, Figure 4e). In the absence of $CO_2/HCO_3^-$ in the media, the same maneuver did not elicit any significant $pH_i$ alteration (Figure 4e). In bicarbonate-free solutions, $\beta_i$ (buffering power) was $27.2\pm3.1$ mmol/l per pH unit in transfected and $28.7\pm3.4$ mmol/l per pH unit in non-transfected cells ($n=3$ for each group, $P>0.05$). In the presence of bicarbonate in the media, the total buffer capacity was $85.4\pm6.1$ mmol/l in transfected and $82.4\pm5.9$ mmol/l in non-transfected cells ($n=3$, $P>0.05$). Taken together, these results are consistent with KBAT functioning in the $Cl^-/HCO_3^-$ exchange mode.

In the last series of experiments, we examined the effect of KBAT on $H^+$-ATPase activity. Toward that end, cultured COS7 cells were plated on coverslips, transiently transfected with KBAT cDNA, and their $pH_i$ was examined 48 h later by the pH-sensitive dye BCECF. To monitor $H^+$ ATPase activity, cells were first acid loaded by $NH_4$ pulse technique and then switched to a hypotonic Na-free solution. Under these conditions, $pH_i$ recovery from intracellular acidosis is exclusively mediated through $H^+$-ATPase as determined by its sodium independence (Figure 5a) and its inhibition in the presence of bafilomycin (ref. 37 and personal observation).

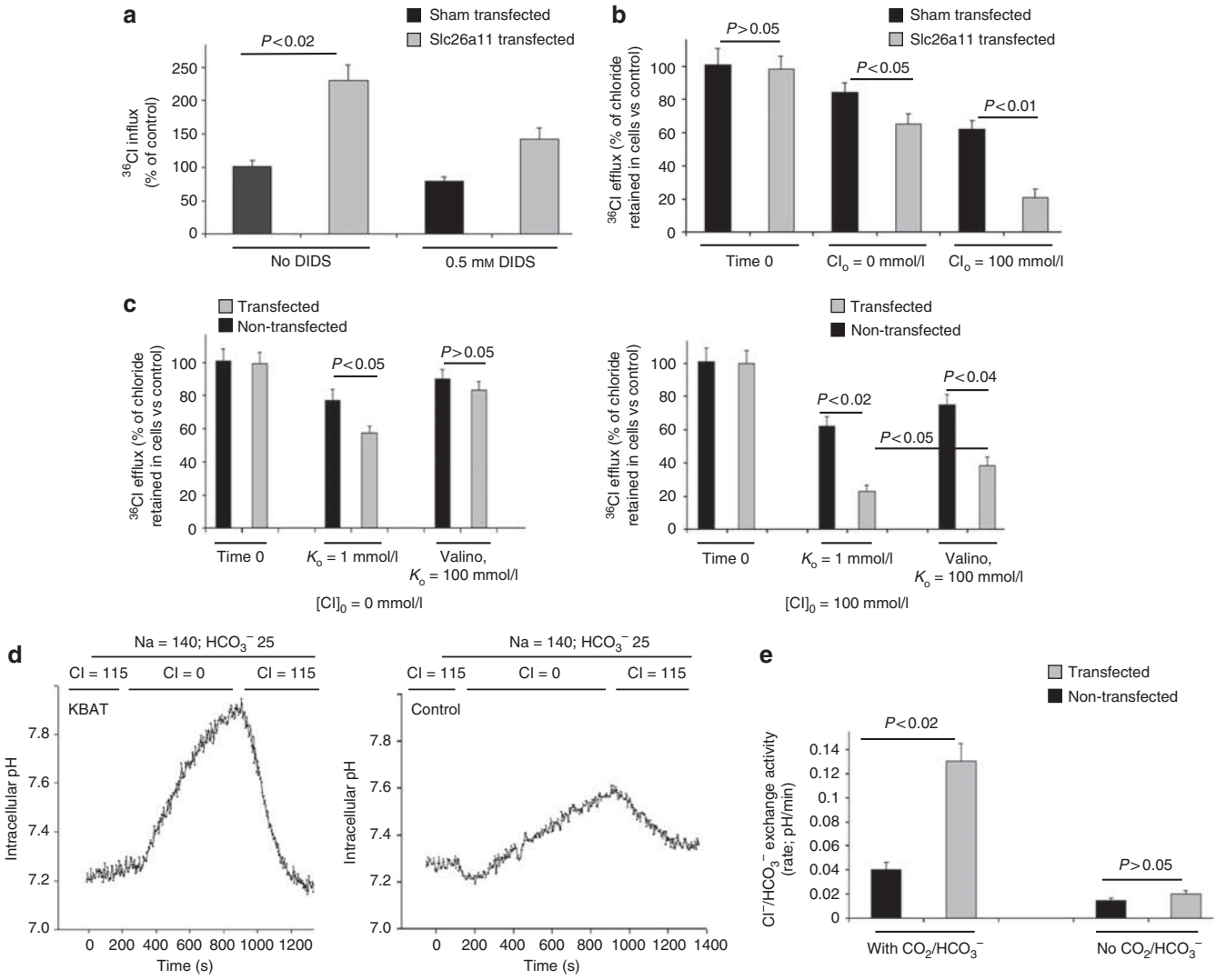


**Figure 4 | Functional identity of Slc26a11 (KBAT).** COS7 cells were transiently transfected with KBAT cDNA and studied by $^{36}Cl$ flux assay (**a–c**) and intracellular pH monitoring (**d** and **e**). (Panel **a**) $^{36}Cl$ influx. Cells were transiently transfected with Slc26a11 (KBAT) cDNA and assayed 48 h later. The influx of 2 mmol/l $^{36}Cl$ was stopped at 10 min using cold saline. The nonspecific Cl uptake (background) was calculated in both transfected and non-transfected cells at time 0 and deducted from their respective 10-min influx values. As shown, cells transfected with KBAT demonstrated significant $^{36}Cl$ influx relative to mock-transfected cells. The presence of DIDS significantly inhibited the $^{36}Cl$ influx. Extracellular $K = 4$mEq. (Panel **b**) $^{36}Cl$ efflux (in the absence or the presence of external chloride). Cells were transiently transfected with Slc26a11 (KBAT) cDNA and assayed 48 h later. Cells were first pre-incubated with 2 mmol/l $^{36}Cl$ for 30 min. Thereafter, the radioactive media were aspirated and cells were washed three times in rapid succession and then incubated with a chloride-free or a chloride-containing solution. The reaction was stopped at time 0 or 10 min. The chloride efflux was calculated as the difference in cell chloride count at time zero (control) and 10 min. As shown, cells transfected with KBAT demonstrated significant amount of $^{36}Cl$ efflux relative to mock-transfected cells, when an outwardly directed potassium gradient (extracellular $K = 1$mEq) was imposed. In the presence of external chloride (100 mmol/l), the rate of $^{36}Cl$ efflux was significantly increased relative to no external chloride. (Panel **c**) Effect of voltage clamping on $^{36}Cl$ efflux in the presence or absence of external chloride. Cells were transiently transfected and then loaded with 2 mmol/l $^{36}Cl$ for 30 min as above. Cells were pre-incubated with 10 μmol/l valinomycin or ethanol (as vehicle). The 10-min efflux of $^{36}Cl$ was assayed in the presence or absence of potassium-rich (100 or 5 mmol/l KCl) solution. The unidirectional chloride efflux by KBAT was abrogated, and the anion exchange mode of KBAT was partially inhibited under voltage-clamped conditions. (Panel **d**) Intracellular $pH_i$ monitoring. $Cl^-/HCO_3^-$ exchanger activity was assayed by subsequent removal and addition of $Cl^-$ as described in the 'Materials and Methods' section. The experiments were repeated in the absence of $CO_2/HCO_3^-$ (see below). Both the intracellular alkalinization upon chloride removal and the $pH_i$ recovery upon switching back to chloride-containing solution were increased in KBAT-transfected cells. In the absence of bicarbonate, the rate of $pH_i$ alteration was minimal in both sham and KBAT-transfected cells (below). (Panel **e**) Summation of $pH_i$ tracing studies. In the presence of $CO_2/HCO_3^-$ in the media, the rate of chloride-dependent bicarbonate transport was significantly increased in KBAT-transfected cells relative to mock-transfected cells. In the absence of $CO_2/HCO_3^-$ in the media, the rate of chloride-dependent $pH_i$ alteration was minimal in both KBAT-transfected and non-transfected cells. Buffering capacity ($\beta_i$) was calculated in mock and KBAT-transfected cells according to established protocols and was not different between the two groups. DIDS, 4,4′-Diisothiocyano-2,2′-stilbenedisulfonic acid; KBAT, kidney brain anion transporter; $pH_i$, intracellular pH; Valino, valinomycin.

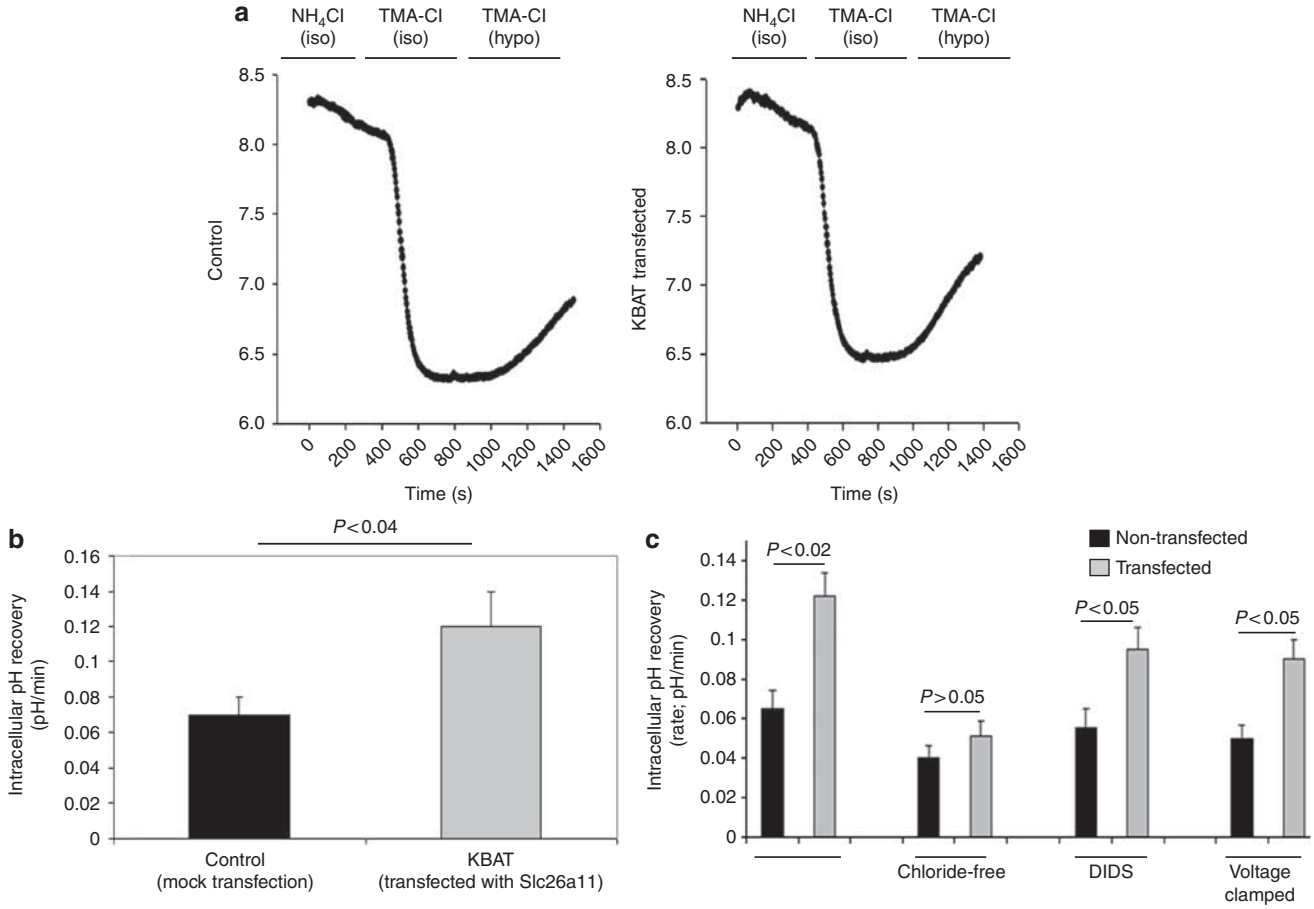


**Figure 5 | Effect of Slc26a11 (KBAT) on $H^+$-ATPase activity (pH studies).** (**a**) Intracellular pH tracing. Cultured COS7 cells were acid loaded with $NH_4+$ pulse in the presence of Na-free (TMA)-Cl. Switching from the isotonic, Na-free solution to hypotonic, Na-free solution resulted in $pH_i$ recovery in mock-transfected, acid-loaded cells (left). KBAT-transfected cells showed a more robust recovery from the acid-loaded state when switched to the hypotonic Na-free solution (right). (**b**) KBAT-transfected vs mock-transfected cells: Summation of results. Summation of recovery rates from acidosis from six separate coverslips showed that $H^+$-ATPase-mediated $pH_i$ recovery from intracellular acidosis was significantly increased in KBAT-transfected cells. (**c**) Characterization of KBAT activation of $H^+$-ATPase. Effect of chloride-free solution on KBAT activated $H^+$-ATPase. Control and KBAT-transfected COS7 cells were acid loaded, depleted of chloride, and then monitored for the recovery from intracellular acidosis in the absence of chloride in the external solution. KBAT stimulation of $H^+$-ATPase activity was almost abrogated in the chloride-depleted state. Effect of DIDS on KBAT activated $H^+$-ATPase. $pH_i$ recovery from intracellular acidosis was monitored in control and KBAT-transfected COS7 cells in the presence of 0.5 mmol/l DIDS added to the external solution. Effect of voltage clamping on KBAT activated $H^+$-ATPase. Control and KBAT-transfected COS7 cells were pre-incubated with valinomycin at 10 μmol/l. Cells were acid loaded and then monitored for recovery from intracellular acidosis in a high-potassium, chloride-containing solution. As shown, KBAT stimulation of $H^+$-ATPase was partially inhibited under voltage clamped conditions. DIDS, 4,4′-Diisothiocyano-2,2′-stilbenedisulfonic acid; KBAT, kidney brain anion transporter; $pH_i$, intracellular pH.

As indicated, KBAT-transfected cells show an $H^+$-ATPase activity, which was significantly increased relative to mock-transfected cells (Figure 5a). The results of six separate experiments demonstrated that the rate of $H^+$-ATPase-mediated acid extrusion increased by ~70% in KBAT-transfected cells ($P<0.03$, $n=6$) (Figure 5b).

To examine the role of KBAT as a chloride transporter on $H^+$-ATPase activity, cells were acid loaded and then assayed for $pH_i$ recovery in a chloride-depleted solution that in addition was sodium free (see the 'Materials and Methods' section). The results demonstrate that $H^+$-ATPase activation by KBAT was almost abolished in chloride-depleted cells (Figure 5c, middle panel vs left panel). As indicated, mock-transfected cells showed moderate inhibition, whereas KBAT-transfected cells showed significant inhibition of $H^+$-ATPase activity under chloride-depleted conditions.

To further ascertain the role of KBAT on $H^+$-ATPase activation, cells were monitored for $pH_i$ recovery from intracellular acidosis as described above in the presence of 0.5 mmol/l DIDS. Our results demonstrate that the rate of Na-independent, bafilomycin-sensitive $pH_i$ recovery from acidosis ($H^+$-ATPase activity) was significantly blunted in cells transfected with KBAT (Figure 5c, right panel vs left panel). As indicated, mock-transfected cells showed mild inhibition, whereas KBAT-transfected cells showed significant inhibition of their $H^+$-ATPase activity by DIDS.

To determine whether KBAT activation of $H^+$-ATPase is mediated through its electrogenic transport of chloride, the experiments were repeated in the presence of high potassium in the perfusion solution (70 mmol/l $K^+$) and valinomycin at 10 μmol/l (Materials and Methods). As shown in Figure 5c (right panel), the dissipation of membrane potential by increased external potassium and valinomycin only partially blocked the stimulation of $H^+$-ATPase by KBAT. Taken together, these results strongly indicate that $H^+$-ATPase activation of KBAT is dependent on intracellular chloride and is partially affected by alterations in membrane potential.

## DISCUSSION

The present studies identify Slc26a11 (KBAT) as a potential functional partner for V $H^+$-ATPase in the kidney collecting duct. KBAT displays remarkable co-localization with $H^+$-ATPase in the kidney collecting duct and is able to transport chloride when expressed in cultured cells. KBAT was able to function as an anion exchanger and as an electrogenic chloride-extruding pathway. KBAT enhanced the $H^+$-ATPase-mediated acid extrusion by a chloride-dependent mechanism in cultured cells.

The kidney collecting duct has an essential role in acid base transport and systemic pH homeostasis. This important function occurs by secretion of acid into the lumen, predominantly by vacuolar $H^+$-ATPase.[28,29] The abundance of vacuolar $H^+$-ATPase in the apical membrane of intercalated cells is mainly controlled by exocytic insertion or endocytic withdrawal of the pump. Studies in various animal models have provided support for this mechanism by showing redistribution of $H^+$-ATPase in the collecting duct in response to increased acid or alkali intake.[37]

Vacuolar $H^+$-ATPase is an electrogenic pump, indicating that its operation creates an electrical potential difference across the membrane. It has been suggested that the continued secretion of acid through $H^+$-ATPase requires that the lumen-positive voltage resulting from electrogenic $H^+$ secretion be dissipated, predominantly by the secretion of an anion (such as $Cl^-$) or by the absorption of a cation (such as $Na^+$).[32,35]

The presence of a chloride channel facilitating the secretion of acid through $H^+$-ATPase in lysosomes, endosomes, and the trans-Golgi network has been well documented.[38–46] The intra-organelle acidification in these compartments by vacuolar $H^+$-ATPase requires the activity of a parallel chloride ion channel to dissipate the membrane potential generated by proton translocation.[38–44]

Recent studies have indicated an important role for chloride in regulating the activity of plasma membrane $H^+$-ATPase in the kidney proximal tubule and the collecting duct. In microperfused rat proximal tubule, intracellular chloride depletion resulted in a significant inhibition of $H^+$-ATPase activity.[34] Studies in microperfused rabbit proximal tubule have shown that chloride depletion or the addition of chloride channel blocker significantly inhibited vacuolar $H^+$-ATPase activity.[33] These results indicate that chloride has an important role in vacuolar $H^+$-ATPase regulation in kidney tubules.[33,34] In microperfused late distal tubule, which expresses electrogenic $H^+$-ATPase and contains intercalated cells, the inhibition of apical $Cl^-$ conductance by 5-nitro-2-(3-phenylpropylamino) benzoic acid (NPPB) significantly altered the luminal membrane potential.[32,45,46] Furthermore, blocking the apical $Cl^-$ conductance reduced the rate of bicarbonate reabsorption in this segment by $>50\%$.[45,46] These results indicate that an apical $Cl^-$ conductance pathway is active and has an important role in acid secretion through $H^+$-ATPase in the collecting duct. However, no studies have identified any chloride transporter/conductance candidate molecule as the functional partner for $H^+$-ATPase in kidney intercalated cells.

It is worth mentioning that the role of chloride in $H^+$-ATPase stimulation is not explained solely by dissipation of a potential difference across the plasma membrane; recent experiments support a direct, specific role of $Cl^-$ in stimulating $H^+$-ATPase activity. These studies have shown that even after dissipating the potential difference across endosome membranes, $H^+$-ATPase still depends on the presence of $Cl^-$ ions. These findings suggest a chloride-binding site in an intra-membrane pump sector.

Our studies indicate that the presence of DIDS significantly inhibited $H^+$-ATPase-mediated acid extrusion in COS7 cells transfected with KBAT (Figure 5c), strongly supporting a regulatory role for KBAT on $H^+$-ATPase activity. Our current results (Figure 5c) further indicate that in the presence of the potassium ionophore valinomycin and a $K^+$-rich external solution, the stimulatory effect of KBAT on $H^+$-ATPase activity remained largely intact. We could not find any significant $Cl^-/H^+$ exchange activity by $pH_i$ monitoring in COS7 cells transfected with KBAT (data not shown); therefore, we do not believe that KBAT is a $Cl^-/H^+$ exchanger.

Our experiments clearly demonstrate the exclusive localization of KBAT in collecting duct intercalated cells (Figures 1–3). Furthermore, our immunolocalization studies unequivocally demonstrate the co-localization of $H^+$-ATPase and KBAT in kidney intercalated cells (Figures 2 and 3). This co-localization has significant functional ramification as shown by enhanced $H^+$-ATPase activity in cells transfected with Slc26a11 (Figure 5).

In addition to the electrogenic chloride transport, KBAT functions as an anion exchanger, both with $^{36}Cl$ flux (Figure 4b and c) and $pH_i$ monitoring methods (Figure 4d and e). This anion exchange mode likely represents a $Cl^-/HCO_3^-$ exchanger (Figure 4d and e). The multi-anion transport capabilities of KBAT is in agreement with properties shown by several other Slc26 family members, and specifically resembles Slc26a9, which can function as an electrogenic $Cl^-/HCO_3^-$ exchanger and as a chloride channel.[9,18,19,21] Given its ability to mediate $Cl^-/HCO_3^-$ exchange and its localization on the basolateral membrane of non-A-intercalated cells in cortical collecting duct (Figure 3),

we propose that KBAT is the basolateral $Cl^-/HCO_3^-$ exchanger in non-A- and non-B-intercalated cells, which are shown to express the $Cl^-/HCO_3^-$ exchanger on both their apical and basolateral membranes.[27–31]

In addition to kidney intercalated cells, bone-resorbing osteoclasts are one of the few mammalian cells that express V $H^+$-ATPase on their apical membrane.[47] Given the remarkable co-localization of $H^+$-ATPase and Slc26a11 in kidney intercalated cells (Figures 1–3) and given the many similarities between the regulatory pathways of $H^+$-ATPase in intercalated cells and osteoclasts,[27,28,47] we entertained the possibility that Slc26a11 is expressed in osteoclasts. Our reverse transcriptase-PCR, northern hybridization, western blotting, and immunofluorescence labeling studies demonstrate that KBAT is abundantly expressed in osteoclasts and co-localizes with $H^+$-ATPase on its ruffled membrane (manuscript in preparation).

KBAT shows abundant expression in the brain and noticeable expression in the distal colon (Figure 1). The cell distribution of KBAT in the brain remains speculative. However, given the expression of $H^+$-ATPase in the brain,[48] it is intriguing to speculate a co-localization and possibly a co-regulation of KBAT and $H^+$-ATPase in brain cells. With regard to the colon, we speculate that this transporter could be expressed on the apical membrane of colonocytes and might have a role in chloride secretion.

In conclusion, Slc26a11 (KBAT) mediates electrogenic transport of chloride, localizes with $H^+$-ATPase in intercalated cells, and facilitates acid secretion. In addition, KBAT can function in the $Cl^-/HCO_3^-$ exchange mode. We propose that Slc26a11 (KBAT) facilitates $H^+$-ATPase-mediated acid secretion in the collecting duct, either by dissipating the membrane potential resulting from $H^+$ secretion with electrogenic chloride transport or directly through mechanism(s) that warrant further examination. In addition, KBAT is likely the basolateral $Cl^-/HCO_3^-$ exchanger in non-A- and non-B-intercalated cells in the cortical collecting duct.

## MATERIALS AND METHODS

### Animal models

C57BL/6 mice at 25–30 g body weight (and Sprague Dawley rats at 150–200 g body weight) were used for these studies. Animals were allowed free access to water and food. The use of anesthetics (pentobarbital sodium) and the method of euthanasia (pentobarbital sodium overdose) were approved according to the institutional guidelines.

### PCR of Slc26a11

Total RNA was prepared from the mouse kidney, poly(A)$^+$-, selected using Oligotex latex beads (Qiagen, Valencia, CA) and then reverse transcribed at 47 °C using SuperScript II RT (Life Technologies, Carlsbad, CA) and oligo(dT) primers. Oligonucleotide primers (5′-TATCATGTCTCTCCTGGTGT CC-sense and 5′-ATCAATTGCAGGGAAGTACAGG-antisense) were designed based on mouse Slc26a11 sequence (GenBank accession number: AF345196). The cycling parameters were 94 °C for 1 min, then 94 °C for 30 s, followed by 68 °C for 2 min for 35 cycles. After PCR, the product was gel purified (revealing a single band of 1.2 kb) and used as a probe for northern blot hybridizations. Sequence analysis of the PCR products verified the sequence as mouse KBAT, which corresponded to the common domain for the short and long variants (see below).

The primers for mouse-specific Slc26a11 variants were as follows: long variant (593 aa), 5′-CTCTGTGAAAGGTCTG GGTC (sense) and 5′-CAGGGCAGGAGATGAAGTC (antisense) (GenBank accession number: AF345196); short variant (420 aa), 5′-GGCCAATTGTCCAGTTACCATG (sense) and GAGGAAAGAGGAGTGGTAGGG (antisense) (GenBank accession number: BC132493). The purified fragments were used as variant specific probes for northern hybridization.

### RNA isolation and northern blot hybridization

Total cellular RNA was extracted from various mouse kidney zones (the cortex, outer medulla, and inner medulla) according to established methods, quantitated spectrophotometrically, and stored at −80 °C. Total RNA samples (30 μg per lane) were fractionated on a 1.2% agarose-formaldehyde gel, transferred to Magna NT nylon membranes, cross-linked by ultraviolet light, and baked. Hybridization was performed according to established methods. The membranes were washed, blotted dry, and exposed to a PhosphorImager screen (Molecular Dynamics, Sunnyvale, CA). Slc26a11 variant-specific $^{32}$P-labeled cDNA fragments (see above) were used as probes for northern hybridizations. The band densities on northern hybridization were quantitated by densitometry using ImageQuaNT software (Molecular Dynamics).

### Cloning of the full-length mouse Slc26a11

Full-length mouse Slc26a11 cDNA (long variant) was amplified from mouse kidney RNA using the following PCR primers: 5′-CTCTGTGAAAGGTCTGGGTC (sense) and 5′-TCAGGGGCCGGAGGGAGACTT (antisense). These primers encode nucleotides 80–1904 of a mouse Slc26a11 cDNA (GenBank accession number: AF345196) and contain the entire open-reading frame. Amplification of the mouse Slc26a11 cDNA by PCR was performed according to the Clontech Advantage 2 PCR kit protocol (Clontech, Mountain View, CA). The product was gel-purified and sequence analysis verified its identity as Slc26a11. The PCR product was ligated into mammalian expression pTarget Vector (Promega, Madison, WI) for expression studies.

### Cell culture and transfection procedures

For transient transfection, the full-length mouse KBAT cDNA, subcloned into a pTarget vector, was used. COS7 cells, grown in 60-mm dishes, were transfected with 8 μg of the full-length KBAT cDNA construct according to established methods.[12,49] Cells were maintained at 37 °C in a 5% $CO_2$:95% $O_2$ air incubator. Northern blots verified strong expression of KBAT in transfected cells. Transient transfection was performed as before[12,49] and cells were examined

48 h after transfection. For experiments, cells were grown either on coverslips or in 24-well plates at 37°C and transfected at 70% confluence with the KBAT expression vector.

#### Antibody generation and immunoblot analysis

A peptide corresponding to aa 274–287 (TRDNKTISF-SEMVQC) of mouse KBAT (GenBank accession number: AF345196) was synthesized and used for antibody generation in two rabbits. The pre-immune and immune sera of the third bleed were purified by IgG purification kit (Sigma, St Louis, MO) and used for immunoblot analysis. Membrane and whole-cell lysates from the kidney cortex were resolved by SDS-PAGE (30 μg per lane) and transferred to nitrocellulose membrane. The membrane was blocked with 5% milk proteins and then incubated for 6 h with 20 μl of KBAT-immune serum diluted at 1:600. The secondary antibody was a donkey anti-rabbit IgG conjugated to horseradish peroxidase (Pierce, Rockford, IL). The site of antigen–antibody complex formation on the nitrocellulose membranes was visualized using chemiluminescence method (SuperSignal Substrate, Pierce) and captured on light-sensitive imaging film (Kodak, Rochester, NY). The antibody against $H^+$-ATPase is a monoclonal antibody against the 31-kDa subunit[37] and a gift from Dr Gluck (through Dr Holliday).[37] The antibody against AQP2[17,50] is a monoclonal antibody and a gift from Dr Ann Blanchard (Paris, France).

#### Immunofluorescence labeling studies

Animals were killed with an overdose of pentobarbital sodium and perfused through the left ventricle with 0.9% saline, followed by cold 4% paraformaldehyde in 0.1 mol/l sodium phosphate buffer (pH 7.4). Kidneys were removed, cut in tissue blocks, and fixed in formaldehyde solution overnight at 4 °C. The tissue was frozen on dry ice, and 6-μm sections were cut with a cryostat and stored at −80 °C until use. Single-immunofluorescence labeling was performed as described previously[16–18] using either Alexa Fluor 488 (green) or Alexa Fluor 594 (red) antibody as secondary antibodies.

For double-immunofluorescence labeling, polyclonal Slc26a11 antibodies were used in conjunction with monoclonal AQP2 or V $H^+$-ATPase at 1:50 dilution. Slc26a11 antibodies were labeled by Alexa Fluor 594 goat anti-rabbit IgG labeling kit and AQP-2, or $H^+$-ATPase antibodies were labeled using Alexa Fluor 488 goat anti-mouse IgG labeling kit (Invitrogen Molecular Probes, Eugene, OR) according to the manufacturer's instructions.

Both frozen and paraffin-embedded sections were used for immunolabeling. For paraffin-embedded sections, we subjected the slides to antigen-retrieval protocol. Frozen kidney sections were allowed to thaw at room temperature and were subsequently rehydrated in phosphate-buffered saline (PBS) for 15 min and permeabilized in PBS containing 0.3% Triton X-100 for 20 min at room temperature. Nonspecific binding was blocked with 1% bovine serum albumin in PBS for 30 min. Zenon labeling complex, which was freshly prepared, was diluted to a final dilution of 1:50 for both primary antibodies and applied to the sections at room temperature for 2 h in a humidified chamber. Sections were thoroughly washed in PBS containing 0.3% Triton X-100 for 10 min three times and then in PBS for 5 min two times. Sections were fixed for the second time in 4% formaldehyde in PBS for 15 min at room temperature. Sections were then washed and mounted in the anti-fade mounting medium (ProLong Antifade Kit from Molecular Probes). Sections were examined and images were acquired on a Nikon PCM 2000 laser confocal scanning microscope (Nikon, Melville, NY) as 0.5-μm 'optical sections' of the labeled cells.

#### $pH_i$ studies

Intracellular pH was monitored using the pH-sensitive fluorescent probe BCECF-acetoxymethyl ester (Molecular Probes), as described previously.[12,35] Cultured COS7 cells were grown on a glass coverslips and transfected with Slc26a11 cDNA and assayed 48 h later. Cells were incubated in the presence of 5 μmol/l BCECF in a $Cl^-$-containing, $HCO_3^-$-free solution consisting of (in mmol/l) 115 NaCl, 25 Na-gluconate, 4 KCl, 1 K-gluconate, and 10 HEPES, at pH 7.4, and gassed with 100% $O_2$. The monolayer was then perfused with the appropriate solutions at 37 °C in a Delta Scan dual excitation spectrofluorometer (PTI, South Brunswick, NJ). For $HCO_3^-$-containing solution, 25 mmol/l Na-gluconate was replaced iso-osmolarly with $NaHCO_3^-$ and gassed with 5% $CO_2$:95% $O_2$. For the $Cl^-$-free solution, all $Cl^-$-containing salts were replaced with gluconate salts. All solutions contained (in mmol/l) 0.8 $K_2HPO_4$, 0.2 $KH_2PO_4$, 1 $CaCl_2$, and 1 $MgCl_2$. For $Cl^-$-free solutions, $CaCl_2$ and $MgCl_2$ were replaced with the gluconate salts. Calibration curves were established by KCl/nigericin.[12,49]

The $Cl^-/HCO_3^-$ exchanger activity was determined by monitoring $pH_i$ alteration in response to sequential switching of the perfusate from chloride containing to chloride free and then back to the chloride-containing solution, as described previously.[12] In experiments in which chloride-free solutions were used, all chloride salts were replaced with equimolar amounts of gluconate. $H^+$-ATPase activity was assayed as the rate of sodium-independent, bafilomycin or concanamycin-sensitive acid extrusion, at isotonic or hypotonic sodium-free solution after acid loading.[51]

#### Buffering power measurement in cultured cells

The intrinsic buffering power ($\beta_i$; $mMH^+$/pH unit) was measured in transfected and non-transfected cultured cells using the $NH_4^+$ pulse method according to the formula $\beta_i = \Delta[NH_4^+]_i/\Delta pH_i$.[51] The experiments were performed in the absence or the presence of $CO_2/HCO_3^-$. Cells were initially incubated in $Na^+$- and $HCO_3^-$-free solution and monitored for $pH_i$ recording. The $Na^+$- and $HCO_3^-$-free solution was similar to the $HCO_3^-$-free solution that was used for the pH studies, except that the NaCl was replaced with iso-osmolar concentration of TMACl (tetramethylammonium chloride). At steady-state $pH_i$, addition of 20 mmol/l

$NH_4Cl$ (20 mmol/l TMACl was replaced with 20 mmol/l $NH_4Cl$) caused a rapid initial increase in cell pH because of the influx of $NH_3$ and subsequent generation of $NH_4^+$. The total buffering capacity in the presence of $HCO_3^-$ ($\beta_T$) was estimated as the sum of $\beta_i$ and the bicarbonate buffer capacity ($\beta_{HCO3-}$).[52]

### Chloride depletion studies

To deplete cells of intracellular chloride, transfected and non-transfected cells were first pulsed with $NH_4Cl$ and then acid loaded by switching to a chloride-free isotonic solution. After generation of intracellular acidosis and achieving the nadir pH, cells were switched to a chloride-free, Na-free hypotonic solution as before. The chloride-free solution was prepared by iso-osmolar replacement of TMACl with TMA-gluconate. Cells were monitored for the Na-independent $pH_i$ recovery as above.

### Voltage clamping studies

Voltage clamp studies were performed by pre-incubating cells with valinomycin (10 μmol/l).[53] The experiments ($^{36}Cl$ efflux or $pH_i$ recovery) were performed in the presence of a potassium-rich solution.

### Radioactive $^{36}Cl$ flux studies

The influx and efflux of $^{36}Cl$ in transfected cultured cells was assayed as before.[54] In brief, cells were pre-loaded with $^{36}Cl$ by pre-incubation with 2 mmol/l $^{36}Cl$ added to a solution that contained 100 mmol/l Na-gluconate, 30 mmol/l K-gluconate, and 10 mmol/l Hepes at pH 7.5 for 60 min. Thereafter, the efflux of $^{36}Cl$ into a low or high potassium-containing solution (1 vs 16 mEq) with or without extracellular chloride (100 vs 0 mmol/l) at normal or pH (7.4) was assayed. The reaction was terminated at 10 min using cold saline, and radioactivity of cells was determined by liquid scintillation spectroscopy.[54] For influx studies, cells were incubated with 2 mmol/l $^{36}Cl$-containing solution and uptake was assayed at 10 min in the presence or the absence of 0.5 mmol/l DIDS.

### Materials

[$^{32}P$]dCTP was purchased from New England Nuclear (Boston, MA). Nitrocellulose filters and other chemicals including valinomycin were purchased from Sigma (St Louis, MO). A RadPrime DNA labeling kit was purchased from Gibco-BRL (Carlsbad, CA). BCECF was obtained from Molecular Probes. A mMESSAGE mMACHINE Kit was purchased from Ambion (Austin, TX).

### Statistical analysis

The results for radioactive flux, northern hybridization, or $pH_i$ studies are presented as means ± s.e. Statistical significance between various experimental groups was determined by ANOVA (analysis of variance) or Student's unpaired *t*-test whenever applicable. $P < 0.05$ was considered significant

### DISCLOSURE

All the authors declared no competing interests.

### ACKNOWLEDGMENTS

These studies were supported by a Merit Review grant from the Department of Veterans Affairs and the National Institute of Health Grant DK 62809 (to MS), and by grants from the US Renal Care, DCA and DCI dialysis care groups (to MS).

### REFERENCES

1. Bissig M, Hagenbuch B, Stieger B *et al.* Functional expression cloning of the canalicular sulfate transport system of rat hepatocytes. *J Biol Chem* 1994; **269**: 3017–3021.
2. Hastbacka J, de la Chapelle A, Mahtani MM *et al.* The diastrophic dysplasia gene encodes a novel sulfate transporter: positional cloning by fine-structure linkage disequilibrium mapping. *Cell* 1994; **78**: 1073–1087.
3. Hoglund P, Haila S, Socha J *et al.* Mutations of the Down-regulated in adenoma (DRA) gene cause congenital chloride diarrhea. *Nat Genet* 1996; **14**: 316–319.
4. Everett LA, Glaser B, Beck JC *et al.* Pendred syndrome is caused by mutations in a putative sulphate transporter gene (PDS). *Nat Genet* 1997; **17**: 411–422.
5. Zheng J, Shen W, He DZ *et al.* Prestin is the motor protein of cochlear outer hair cells. *Nature* 2000; **405**: 149–155.
6. Lohi H, Kujala M, Kerkela E *et al.* Mapping of five new putative anion transporter genes in human and characterization of SLC26A6, a candidate gene for pancreatic anion exchanger. *Genomics* 2000; **70**: 102–112.
7. Lohi H, Kujala M, Makela S *et al.* Functional characterization of three novel tissue-specific anion exchangers SLC26A7, -A8, and -A9. *J Biol Chem* 2002; **277**: 14246–14254.
8. Vincourt JB, Jullien D, Amalric F *et al.* Molecular and functional characterization of SLC26A11, a sodium-independent sulfate transporter from high endothelial venules. *FASEB J* 2003; **17**: 890–892.
9. Romero MF, Chang MH, Plata C *et al.* Physiology of electrogenic SLC26 paralogues. *Novartis Found Symp* 2006; **273**: 126–138.
10. Soleimani M, Xu J. SLC26 chloride/base exchangers in the kidney in health and disease. *Semin Nephrol* 2006; **26**: 375–385.
11. Melvin JE, Park K, Richardson L *et al.* Mouse down-regulated in adenoma (DRA) is an intestinal Cl(-)/HCO(3)(-) exchanger and is upregulated in colon of mice lacking the NHE-3 Na(+)/H(+) exchanger. *J Bio Chem* 1999; **274**: 22855–22861.
12. Soleimani M, Greeley T, Petrovic S *et al.* Pendrin: an apical Cl-/OH-/HCO3-exchanger in the kidney cortex. *Am J Physiol Renal Physiol* 2001; **280**: F356–F364.
13. Petrovic S, Ju X, Barone S *et al.* Identification of a basolateral Cl-/HCO3-exchanger specific to gastric parietal cells. *Am J Physiol Gastrointest Liver Physiol* 2003; **284**: G1093–G1103.
14. Verlander JW, Hassell KA, Royaux IE *et al.* Deoxycorticosterone upregulates PDS (Slc26a4) in mouse kidney: role of pendrin in mineralocorticoid-induced hypertension. *Hypertension* 2003; **179**: 356–362.
15. Schweinfest CW, Spyropoulos DD, Henderson KW *et al.* Slc26a3 (dra)-deficient mice display chloride-losing diarrhea, enhanced colonic proliferation, and distinct up-regulation of ion transporters in the colon. *J Biol Chem* 2006; **281**: 37962–37971.
16. Wang Z, Wang T, Petrovic S *et al.* Renal and intestine transport defects in Slc26a6-null mice. *Am J Physiol Cell Physiol* 2005; **288**: C957–C965.
17. Xu J, Song P, Nakamura S *et al.* Deletion of the chloride transporter slc26a7 causes distal renal tubular acidosis and impairs gastric acid secretion. *J Biol Chem* 2009; **284**: 29470–29479.
18. Xu J, Song P, Miller ML *et al.* Deletion of the chloride transporter Slc26a9 causes loss of tubulovesicles in parietal cells and impairs acid secretion in the stomach. *Proc Natl Acad Sci USA* 2008; **105**: 17955–17960.
19. Chang MH, Plata C, Zandi-Nejad K *et al.* Slc26a9—anion exchanger, channel and Na+ transporter. *J Membr Biol* 2009; **228**: 125–140.
20. Kim KH, Shcheynikov N, Wang Y *et al.* SLC26A7 is a $Cl^-$ channel regulated by intracellular pH. *J Biol Chem* 2005; **280**: 6463–6470.
21. Dorwart MR, Shcheynikov N, Wang Y *et al.* SLC26A9 is a $Cl^-$ channel regulated by the WNK kinases. *J Physiol* 2007; **584**: 333–345.
22. Xie Q, Welch R, Mercado A *et al.* Molecular characterization of the murine Slc26a6 anion exchanger: functional comparison with Slc26a1. *Am J Physiol Renal Physiol* 2002; **283**: F826–F838.
23. Jiang Z, Grichtchenko II, Boron WF *et al.* Specificity of anion exchange mediated by mouse Slc26a6. *J Biol Chem* 2002; **277**: 33963–33967.
24. Clark JS, Vandorpe DH, Chernova MN *et al.* Species differences in Cl- affinity and in electrogenicity of SLC26A6-mediated oxalate/

Cl- exchange correlate with the distinct human and mouse susceptibilities to nephrolithiasis. *J Physiol* 2008; **586**: 1291–1306.
25. Freel RW, Hatch M, Green M *et al.* Ileal oxalate absorption and urinary oxalate excretion are enhanced in Slc26a6 null mice. *Am J Physiol Gastrointest Liver Physiol* 2006; **290**: G719–G728.
26. Jiang Z, Asplin JR, Evan AP *et al.* Calcium oxalate urolithiasis in mice lacking anion transporter Slc26a6. *Nat Genet* 2006; **38**: 474–478.
27. Blake-Palmer KG, Karet FE. Cellular physiology of the renal H+ATPase. *Curr Opin Nephrol Hypertens* 2009; **18**: 433–438. Review.
28. Brown D, Paunescu TG, Breton S *et al.* Regulation of the V-ATPase in kidney epithelial cells: dual role in acid-base homeostasis and vesicle trafficking. *J Exp Biol* 2009; **212**: 1762–1772. Review.
29. Schwartz GJ, Barasch J, Al-Awqati Q. Plasticity of functional epithelial polarity. *Nature* 1985; **318**: 368–371.
30. Alper SL, Natale J, Gluck S *et al.* Subtypes of intercalated cells in rat kidney collecting duct defined by antibodies against erythroid band 3 and renal vacuolar H+-ATPase. *Proc Natl Acad Sci USA* 1989; **86**: 5429–5433.
31. Valles P, Lapointe MS, Wysocki J *et al.* Kidney vacuolar H+ -ATPase: physiology and regulation. *Semin Nephrol* 2006; **26**: 361–374. Review.
32. Carraro-Lacroix LR, Lessa LM, Fernandez R *et al.* Physiological implications of the regulation of vacuolar H+-ATPase by chloride ions. *Braz J Med Biol Res* 2009; **42**: 155–163.
33. Malnic G, Geibel JP. Cell pH and H(+) secretion by S3 segment of mammalian kidney: role of H(+)-ATPase and Cl(-). *J Membr Biol* 2000; **178**: 115–125.
34. Wagner CA, Giebisch G, Lang F *et al.* Angiotensin II stimulates vesicular $H^+$-ATPase in rat proximal tubular cells. *Proc Natl Acad Sci USA* 1998; **95**: 9665–9668.
35. Tararthuch AL, Fernandez R, Malnic G. $Cl^-$ and regulation of pH by MDCK-C11 cells. *Braz J Med Biol Res* 2007; **40**: 687–696.
36. Hilden SA, Johns CA, Madias NE. Cl(-)-dependent ATP-driven $H^+$ transport in rabbit renal cortical endosomes. *Am J Physiol* 1988; **255**: F885–F897.
37. Bastani B, Purcell H, Hemken P *et al.* Expression and distribution of renal vacuolar proton-translocating adenosine triphosphatase in response to chronic acid and alkali loads in the rat. *J Clin Invest* 1991; **88**: 126–136.
38. Wada Y, Ohsumi Y, Anraku Y. Chloride transport of yeast vacuolar membrane vesicles: a study of *in vitro* vacuolar acidification. *Biochim Biophys Acta* 1992; **1101**: 296–302.
39. Gerencser GA, Zhang J. Existence and nature of the chloride pump. *Biochim Biophys Acta* 2003; **1618**: 133–139. Review.
40. Glickman J, Croen K, Kelly S *et al.* Golgi membranes contain an electrogenic H+ pump in parallel to a chloride conductance. *J Cell Biol* 1983; **97**: 1303–1308.
41. Xie XS, Stone DK, Racker E. Determinants of clathrin-coated vesicle acidification. *J Biol Chem* 1983; **258**: 14834–14838.
42. Arai H, Pink S, Forgac M. Interaction of anions and ATP with the coated vesicle proton pump. *Biochemistry* 1989; **28**: 3075–3082.
43. Jentsch TJ. Chloride and the endosomal-lysosomal pathway: emerging roles of CLC chloride transporters. *J Physiol* 2007; **578**(Part 3): 633–640.
44. Smith AJ, Schwappach B. Cell biology: think vesicular chloride. *Science* 2010; **328**: 1364–1365.
45. Malnic G, Fernandez R, Cassola AC *et al.* Mechanisms and regulation of H+ transport in distal tubule epithelial cells. *Wien Klin Wochenschr* 1997; **109**: 429–434.
46. Fernández R, Bosqueiro JR, Cassola AC *et al.* Role of Cl- in electrogenic H+ secretion by cortical distal tubule. *J Membr Biol* 1997; **157**: 193–201.
47. Cipriano DJ, Wang Y, Bond S *et al.* Structure and regulation of the vacuolar ATPases. *Biochim Biophys Acta* 2008; **1777**: 599–604.
48. Mooradian AD, Bastani B. Identification of proton-translocating adenosine triphosphatases in rat cerebral microvessels. *Brain Res* 1993; **629**: 128–132.
49. Burnham CE, Amlal H, Wang Z *et al.* Cloning and functional expression of a human kidney Na+:HCO3- cotransporter. *J Biol Chem* 1997; **272**: 19111–19114.
50. Barone S, Amlal H, Kujala M *et al.* Regulation of the basolateral chloride/base exchangers AE1 and SLC26A7 in the kidney collecting duct in potassium depletion. *Nephrol Dial Transplant* 2007; **22**: 3462–3470.
51. Amlal H, Goel A, Soleimani M. Activation of H+-ATPase by hypotonicity: a novel regulatory mechanism for H+ secretion in IMCD cells. *Am J Physiol* 1998; **275**: F487–F501.
52. Roos A, Boron WF. Intracellular pH. *Physiol Rev* 1981; **61**: 296–434.
53. Krick S, Platoshyn O, Sweeney M *et al.* Activation of K+ channels induces apoptosis in vascular smooth muscle cells. *Am J Physiol Cell Physiol* 2001; **280**: C970–C979.
54. Soleimani M, Howard RL. Presence of chloride-formate exchange in vascular smooth muscle and cardiac cells. *Circ Res* 1994; **74**: 48–55.